Patterns and trends of ozone and carbon monoxide at Ushuaia (Argentina) observatory

J.A. Adame [a,*], O. Puentedura [b], L. Gómez [b], L. Condorí [c], G. Carbajal [d,e], M.E. Barlasina [f], M. Yela [b]

[a] *Atmospheric Sounding Station, El Arenosillo observatory, Atmospheric Research and Instrumentation Branch, National Institute for Aerospace Technology (INTA), Mazagón-Huelva, Spain*
[b] *Atmospheric Research and Instrumentation Branch, National Institute for Aerospace Technology (INTA), Torrejón de Ardoz, Madrid, Spain*
[c] *Ushuaia GAW Station, National Meteorological Service (SMN), Ushuaia, Argentina*
[d] *National Meteorological Service (SMN), Atmospheric Watch and Geophysical (GIDyC – VAYGEO), Buenos Aires, Argentina*
[e] *Pontificia Universidad Católica Argentina, PEPACG, Facultad de Ingeniería y Ciencias Agrarias, Buenos Aires, Argentina*
[f] *Meteorological Service (SMN), Atmospheric Watch and Geophysical (GIDyC–VAYGEO), Buenos Aires, Argentina*

ARTICLE INFO

ABSTRACT

The behavior patterns for surface ozone (O_3) and carbon monoxide (CO) were investigated with the hourly mixing ratios registered for nine years (2010 to 2018) at the GAW-WMO (Global Atmospheric Watch – World Meteorological Organization) station of Ushuaia (Argentina). Two behavior patterns were identified for these species after applying a criterion. Specific periods were analyzed in detail, in which nitrogen dioxide (NO_2) was also studied. The weather conditions were explored using the ERA5 meteorological fields from the ECMWF (European Centre for Medium-Range Weather Forecasts). Outputs of the chemical transport model from the Copernicus Atmosphere Monitoring Service (CAMS) were used to investigate the spatial distribution of O_3, CO and NO_2. The more frequent scenario is characterized by the unaltered mixing ratios of O_3 and CO for days, with values of 10–15 ppb and 60–70 ppb, respectively, and below 200 ppt for NO_2. This pattern occurred with intense westerly airflows associated with the low-pressure system located in the south of the Pacific Ocean. A second pattern was observed in 45.8 ± 3.4% of the days, which was characterized by low O_3 mixing ratios (~12 ppb), high NO_2 concentrations (above ~3000 ppt) and CO peaks exceeding 400 ppb. This scenario was defined by a high-pressure system blocking the westerly winds, which results in atmospheric stagnation and in the accumulation of trace gases in the lower layers. Finally, the annual trend was explored; no O_3 trend was obtained, although an unexpected upward CO trend was identified, with an increase of 1.75 ± 0.49 ppb year^{-1}. To investigate its causes, the annual evolution of the temperature at 850 hPa level (T850) and geopotential height at 500 hPa level (Z500) anomalies along with the CO emissions were analyzed. While no trends were found in weather conditions, the CO emissions showed an increasing trend of 4.4% year^{-1}; therefore, the CO increase could be attributed to the emission changes. In the future, warm climate with more frequent anticyclonic situations, together with a growing trend in emissions, could lead to a drastic change in the current levels of these trace gases, in remote regions such as Ushuaia.

1. Introduction

Surface and tropospheric ozone (O_3) is a major air pollutant harmful to human health and to terrestrial vegetation. Ozone pollution is a serious concern in many places around the world (Li et al., 2019), affecting rural and remote areas (Pires et al., 2012). O_3 is a secondary species formed in the atmosphere from precursors such as nitrogen oxides ($NO_x = NO_2 + NO$), volatile organic compounds (VOCs), carbon monoxide (CO), and methane (CH_4) in the presence of sunlight. In recent decades, a clear upward trend has been observed in many regions of the planet (Cooper et al., 2014, 2020), and it is a reactive and greenhouse gas considered as a climate forcer (Monks et al., 2015).

Carbon monoxide (CO) is also a reactive gas, emitted to the atmosphere by both natural and anthropogenic sources, such as biomass

---

burning and fossil fuel burning. Transportation and biomass burning are the largest contributors to anthropogenic emissions of CO. This gas has adverse human health effects, being lethal in high concentrations (>1000 ppm), although it also causes health problems in lower concentrations. CO contributes to positive radiative forcing (warming) through its role in ozone production, as well as through an increase in methane lifetime (von Schneidemesser et al., 2015).

Nitrogen dioxide (NO_2) is one of the so-called nitrogen oxides (NO_x sum of NO plus NO_2), which are primarily emitted to the atmosphere during fossil fuel combustion, and is a key species in the formation of surface O_3. In addition, NO_2 is considered to be an important air pollutant in industrial and metropolitan areas (Kang et al., 2019).

Previous works on O_3 and CO in the southern region of South America are relatively scarce, although in recent years some studies have been carried out, mainly focused on the analysis of O_3 exceedances in Santiago de Chile (Seguel et al., 2020), air pollution in the central zone of Chile (Toro et al., 2015) and O_3 trends in El Tololo observatory (Anet et al., 2017).

In a changing global atmosphere, changes in the weather patterns and in the chemical composition are strongly linked. Although these changes are taking place on a global scale, there are specific places which could be defined as hot-spots, such as deserts (Magee, 2016), large forest areas like the Amazon, Alaska (Flannigan et al., 2009) and the Polar Regions, both the Arctic, where the phenomenon defined as Arctic Amplification is well known (Coumou et al., 2018), and the Antarctic and its adjacent regions, which are more sensitive to these changes.

Ushuaia, although it is located in the continent of America, is located in a Subantarctic region, which makes it a suitable place to observe and detect changes in weather patterns, concentration levels and behavior of trace gases. In fact, the Ushuaia atmospheric observatory belongs to the GAW program of the WMO. Therefore, the Ushuaia measurements (mainly O_3) were used in general studies (Cooper et al., 2014, 2020; Parrish et al., 2016). However, specific studies are necessary to identify not only the trends but also their origin and to investigate the link between changing weather conditions and dynamic and chemical processes of the trace gases. With this goal, in a previous work (Adame et al., 2019) was carried out a detailed studied to know the weather conditions in this region, the atmospheric transport processes and the daily and monthly evolutions of the O_3 and CO. The horizontal distribution for O_3 and CO was also investigated with satellite observations.

This work aims to identify and analyze the behavior patterns shown by two trace gases, O_3 and CO, in this remote environment by using measurements collected for a period of nine years at the GAW Ushuaia station. Moreover, and despite the fact that it is a short period, the trends depicted by these gases were also explored.

2. Experimental conditions and methods

2.1. Measurement site

The Ushuaia region is located at the south of Argentina, in the province of Tierra del Fuego, surrounded by the Martial mountain range (to the north, east and west), which is one of the last sections of the Andes mountains. The city is situated in the coast of the Isla Grande de Tierra del Fuego, with the bay and the Beagle channel in the south. In this zone, and approximately 5 km away from the city, the GAW Ushuaia observatory ($54°\ 50'$ S - $68°\ 18'$ W) is located, a few metres from a coastal cliff and 17 m above sea level (a.s.l.) (Fig. 1a).

2.2. Instrumentation to measure trace gases (O_3, CO and NO_2) and local meteorology

In this work, O_3, CO and NO_2 experimental data were used. For O_3 and CO, the data had a temporal resolution of one minute. The air inlet system has an air intake 7 m above ground level (a.g.l.) over the
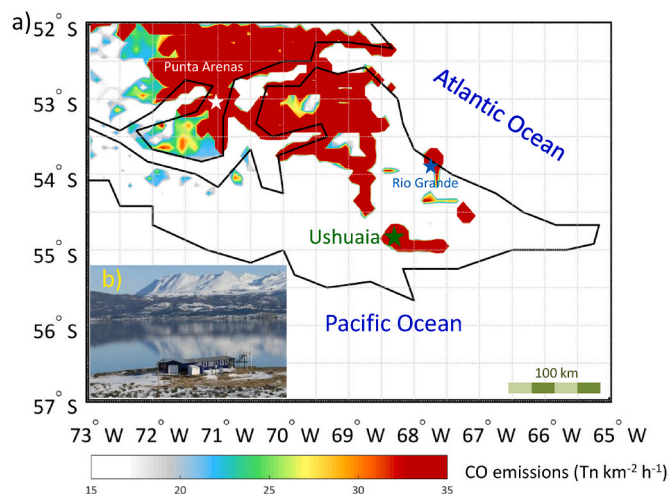

Fig. 1. Spatial distribution of the emission sources for CO (in Tn $km^{-2}\ h^{-1}$) in 2018 obtained from the Copernicus emission inventory, with a spatial resolution of $0.1^0 \times 0.1^0$. Location of Ushuaia, Rio Grande and Punta Arenas (stars) (a) and image of the GAW Ushuaia observatory (b).

observatory roof with continuous flow at 11 l min^{-1}. O_3 was measured by UV absorption using a TEI 49C (Thermo Electron Corporation, Environmental Instruments) analyzer. An automatic calibration is carried out daily, which consists of circulating air-zero cylinder (ozone-free air) during 55 min. Monthly maintenance is performed that consists of checking the filters and checking the instrument for leaks. Every four months, a manual span calibration with three points (10, 50 and 100 ppb) was carried out. In addition, it was calibrated by a UV photometric calibrator (TEI Model 49PS) approximately every six months. The O_3 instrument participated in comparison campaigns in 2010 and 2017, in the Regional Calibration Center of Buenos Aires (RCC-Surface Ozone) and WMO (WMO, 2010; 2017b). Also, the instrument was audited at the GAW Ushuaia station since 2016 and 2019 (WMO, 2016, 2019b).

CO was measured by nondispersive IR absorption photometry (NDIR) using a HORIBA (APMA–360). Every day, it performs a calibration that consists of circulating air-zero cylinder (carbon monoxide-free air) through the analyzer for 43 min, then 15 min with a dilution between CO of 98,800 ppb and air-zero, to obtain a dilution of 400 ppb with 3 l min^{-1} flow. Monthly, the maintenance is performed that consists of checking the filters, and then circulating air-zero for 20 min with a specific concentration of 2582 ppb. Every six months, a calibration with three points (200, 500 and 800 ppb) was performed. Similar to O_3, CO was also audited at the GAW Ushuaia station since 2016 and 2019. The hourly values were obtained from the data recorded every minute.

NO_2 measurements were performed using a MAXDOAS (Multi Axis Differential Optical Absorption Spectroscopy) instrument. MAXDOAS is a well-known technique commonly used to retrieve tropospheric components based on DOAS technique (Platt and Stutz, 2008). The MAX-DOAS instrument deployed at Ushuaia was fully developed by INTA in the framework of their Antarctic program of measurements. This program was established in 1994 and is devoted to the measurement of the change in the Antarctic atmospheric composition (Yela et al. 2017, Prados-Roman et al., 2018). This instrument was settled at Ushuaia GAW station in 2015 and consists of an outdoor light collector pointing at 247° N in azimuth direction, composed of a thermostatized pointer and a telescope with 1° FOV. The skylight is guided through an optics fibre bundle to the indoor unit, which consists of a Czerny-Turner spectrograph and a CCD (Charge-Coupled Device) camera based on a HAMAMATSU S7031–1008 sensor, located in a temperature controlled box. MAXDOAS measurements were performed in cycles of about 15 min, scanning at elevations from horizon to zenith, with a solar zenith angle below 85°.

MAXDOAS retrieval of NO_2 was performed according to the recommendations of Peters et al. (2017). In this work, the zenith and horizontal view of each cycle was used to estimate the NO_2 concentration at the level of the station following the technique described by Gomez et al. (2014). NO_2 Volume Mixing Ratio (VMR) was calculated using O_4 differential slant column density to estimate the optical path along the horizontal view. O_4 is the collision complex of O_2, whose concentration and distribution is well known in the atmosphere, which can be retrieved from MAXDOAS measurements in the visible spectrum. The optical path to retrieve VMR from MAXDOAS measurements can be then obtained by estimating the concentration of O_2 in the atmosphere and using the values of O_4 slant column density from these measurements. The standard AFGL (Air Force Geophysics Laboratory) profile of temperature and pressure for a Subarctic latitude (Anderson et al., 1986) was used to obtain the O_2 concentration in the horizontal path and the optical path at elevation 0° (instrument pointing to the horizon).

Finally, the local meteorology, temperature and wind (direction and speed) were used in this work. A Väisala weather automatic station at 2 m a.g.l. was used to measure temperature, while a Young instrument on a 10 m mast was used to measure the wind. All the parameters were recorded with one-minute temporal resolution.

2.3. Retrieval of NO_2 vertical profile from MAXDOAS instrument

Vertical profiles of NO_2 mixing ratios can be estimated from NO_2 MAXDOAS differential slant columns densities (DSCDs) obtained at different elevation angles using the Optimal Estimation Method (OEM) (Rodgers, 2000) and Radiative Transfer models (RTM). This method was previously validated in Tirpitz et al. (2020). In a first step, aerosol vertical profiles were obtained through a non-linear iterative process from MAXDOAS O_4 DSCDs recorded simultaneously with those of NO_2. Once the aerosols were estimated, the NO_2 vertical profiles were obtained using the estimated aerosol profiles as input in the RTM.

In this work, aerosol and NO_2 profiles were obtained with bePro OEM retrieval code (Clémer et al., 2010), based on LIDORT RTM (Spurr, 2008). The calculations must consider surface albedo, state of the atmosphere, optical properties of the main present absorbing/scattering species and a vertical a priori distribution of the study species. Aerosols optical properties are modelled through Henyey–Greenstein phase functions for single scattering albedo SSA = 0.999982 and asymmetry parameter g = 0.89 (Dominé et al., 2008). Given that the MAXDOAS spectrometer looks torwards the ocean, a surface albedo of 0.07, typical of oceanic surface (Roesch et al., 2002), was considered. Aerosol and NO_2 a priori profiles are considered typical, exponentially decreasing functions with a scale height of 1 km. Corresponding surface values of these profiles are 0.02 km^{-1} for aerosols and 1 ppb for NO_2. DSCD for zero elevation is affected by an obstacle, thus only DSCDs corresponding to elevation angles between 1 and 90° were taken into account.

2.4. Global meteorological and chemical transport models and emission inventory

To investigate the weather conditions at the Ushuaia region, mean sea level pressure (MSLP) and wind fields from the global ECMWF (European Centre for Medium Range Weather Forecasts) model were used, specifically the ERA5 data reanalysis (Hersbach and Dee, 2016). ERA5 was produced using 4D-Var data assimilation in CY41R2 of ECMWF's Integrated Forecast System (IFS), with 137 hybrid sigma/pressure (model) levels in the vertical, with the top level at 0.01 hPa. The IFS is coupled to a soil model, the parameters of which are also designated as surface parameters, and an ocean wave model. The ERA5 dataset contains one high-resolution realization (HRES), which has a resolution of 31 km (0.28125°). Depending on the parameter, the data are archived either as spectral coefficients with a triangular truncation of T639 (HRES) and T319 (EDA) or on a reduced Gaussian grid with a resolution of N320 (HRES) N160 (EDA). The sub-daily data for the HRES

analyses are available hourly (C3S 2017). Using hourly output meteorological fields (https://cds.climate.copernicus.eu), synoptic maps were plotted. To explore the vertical structure of the first kilometers of the atmosphere, hourly values of the atmospheric boundary layer (ABL) height were also extracted in a specific period. The boundary layer height is calculated using an algorithm based on the bulk Richardson (R_i) number (Vogelezang and Holtslag, 1996), being defined as the lowest level at which the bulk R_i reaches the critical value of 0.25 (ECMWF, 2017).

Since ERA5 data reanalysis from 1979 are currently available, the monthly mean values for temperature and geopotential height at the pressure levels of 850 and 500 hPa were used, obtaining the annual averages for Ushuaia. To explore possible changes in the synoptic conditions during the study period, the anomalies of these two parameters were calculated. The climatological series of 1981–2010 was considered as the reference period.

The CAMS global near real-time (NRT) provides daily analyses and forecasts of trace gas and aerosol concentrations with the Composition-IFS system, with data assimilation of trace gas mixing ratios and aerosol properties (Huijnen et al., 2016). CO, O_3 and NO_2 fields were extracted from the CAMS–NRT mode at the 1000 hPa pressure level, with a time step of 3 h and spatial resolution of 0.25° x 0.25° (latitude x longitude).

To investigate the temporal evolution of the CO emissions at the Ushuaia region, the CAMS global and regional emission inventory (Granier et al., 2019) was used. To have an accurate quantification of surface emissions from anthropogenic and natural sources, the CAMS global anthropogenic emissions, which are based on the emissions provided by the EDGARv4.3.2 inventory developed by the European Joint Center (Crippa et al., 2018) and the Community Emissions Data System emissions (Hoesly et al., 2018), were used. Annual averages with 0.1° x 0.1° as spatial resolution were used in this study.

2.5. Criteria to identify O_3 and CO patterns

Previous studies (Adame et al., 2019) show the occurrence of two main patterns of CO and O_3 at the Ushuaia region. The first pattern is characterized by almost constant O_3 and CO mixing ratios under conditions governed by the synoptic scale, which is described in detail in section 3.2; the second pattern is governed by the local scale and distinguished by an increase in the CO values along with a drop in the ozone mixing ratios, in the Fig. 6 the two mentioned O_3-CO patterns are shown. To later identify and analyze these patterns, two criteria were applied to the hourly database: for the identification of the first pattern, the condition imposed was that the mixing ratio of O_3 and CO did not vary more than 10% for at least 24 h. In the second case, a selected day was considered to follow this pattern if there was, simultaneously in one hour, a decrease of 20% in the O_3 level and an increase of 30% for CO with respect to the values observed two hours before. An event day was considered if at least two consecutive hours met this double criterion. Although other criteria may be applied, the previous visualization of the O_3 and CO time series showed that, by applying the aforementioned criteria, they were restrictive enough to capture all events.

3. Results

3.1. Ozone and carbon monoxide overview and emission sources

During the nine-year measurements period, an absolute maximum of 40 ppb was obtained for O_3, measured on June 30th 2010 at 19:00 UTC, with a 95th percentile of 32.1 ppb, a mean of 20.3 ± 7.6 ppb and a median of 19.8 ppb; the lowest mixing ratios were 8.0 ppb as the 5th percentile. For CO, there were two remarkable absolute maxima recorded in these nine years: the one collected on May 26th 2015 at 23:00 had an hourly value of 735 ppb, and the one collected on August 24th 2014 at 2:00 UTC had a mixing ratio of 654 ppb. Both CO peaks were unexpected for this background environment. While the 95th percentile was

164.5 ppb, the mean was 72.9 ± 47.5 and the median was 59.6 ppb. The difference with the mean could be associated with the highest CO values. Considering the CO baseline as the 5th percentile, a value of 40.7 ppb was obtained.

O_3 and CO at the Ushuaia region show monthly and diurnal variations. For O_3, the minima were observed in the summer months, while the maxima were observed in the winter months. A similar pattern was found for CO. Regarding daily evolutions, O_3 and CO presented nearly constant mixing ratios during the day, although in the case of O_3 there was a slight increase at midday. These temporal evolutions were studied in detail in Adame et al. (2019).

The patterns of O_3 and CO would be modulated by both weather conditions and emissions sources. Since the meteorological factor is presented in the next section, the possible emissions sources, which affect the Ushuaia region, were investigated. Previously, it is well known that the main atmospheric emissions at Ushuaia could be associated with the fossil fuel burned for domestic heating, transportation and power generation. The Copernicus emission inventory was used to investigate the temporal evolution of these emissions using CO as tracer of the representative emissions in this area.

Fig. 1 shows the horizontal distribution of the total CO emissions, including all the sources, in 2018. The Ushuaia city can be clearly

considered as the closest source emission, and, consequently, the chemical measurements collected at the station could be affected by this source. Its degree of influence depends fundamentally on the wind (direction and speed) on a horizontal scale, as well as on the ABL structure in the vertical component.

Other remote sources that could affect the station are located NW, the same direction in which the Martial mountain range is located. One of them is an extensive region in the north of Isla Grande de Tierra del Fuego, approximately 100–120 km from Ushuaia, where the city of Río Grande, located in the coastal zone, is found, in which there are industrial activities for the extraction of gas and oil from the deposits located in the region. The second remote source with the highest CO emission levels of this region is the city of Punta Arenas (Chile); although located 250 km NW of Ushuaia, with favorable airflows from this direction, its emissions could affect not only the Ushuaia but the whole Tierra del Fuego region.

3.2. O_3 and CO pattern under weather conditions governed by westerly winds

As mentioned in Section 2.5, the first investigated scenario is governed by the synoptic scale. The weather conditions at the Ushuaia
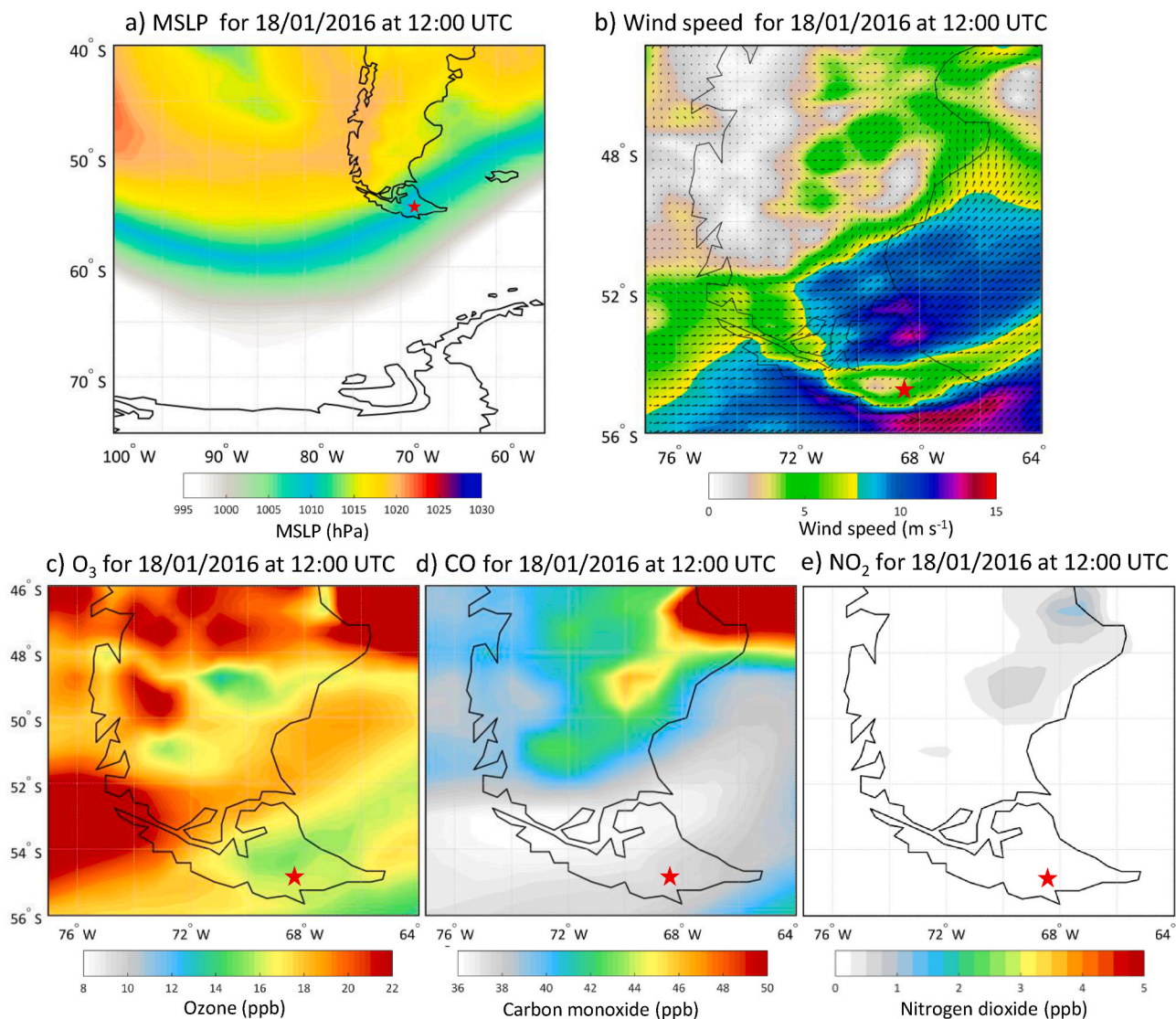

Fig. 2. Mean sea level pressure (MSLP) and wind fields for January 18th 2016 at 12:00 UTC (a-b), and CO, O_3 and NO_2 spatial distribution obtained from the CAMS model with a $0.25^0 \times 0.25^0$ spatial resolution (c-d-e). Location of Ushuaia (star).

region are mostly governed by westerly airflows that are caused by an almost permanent low-pressure system located in the Pacific Ocean, in the west of the Antarctic Peninsula, affecting the Bellingshausen and Amundsen seas at latitudes below 65^0 S. Weather is also strained by the high-pressure system also located in the Pacific Ocean but at higher latitudes, approximately between 40^0 and 50^0 S. The Ushuaia and Tierra del Fuego regions are situated in a transition zone between these two high and low-pressure systems, a corridor influenced by these intense winds at any season of the year (Fig. 2a).

Although many periods with these same characteristics were identified and analyzed, the period January 16th–20th 2016 (summer season) was selected as representative for this work. To investigate the weather conditions, hourly MSLP and wind fields obtained from a reanalysis of the ERA5 data were used (Fig. 2a-b). The MSLP map revealed an isobaric configuration, as previously mentioned, while the wind fields showed intense westerly airflows in the entire zone of Tierra del Fuego, with wind speeds higher than 10–12 m s^{-1}. The local wind supported the results obtained with ERA5: constant flows blowing from SW-W with wind speeds higher than 6 m s^{-1} and gust higher than 15 m s^{-1} (Fig. 3a).

Under these conditions, O_3 and CO measurements on the surface showed values that were almost constant for two consecutive days. In the summer months, the mixing ratios showed ranges of 10–15 ppb and 60–70 pbb for O_3 and CO, respectively, while NO_2 registered values below 80 ppt (Fig. 3bc). Although it is not shown, this pattern was also observed during the winter months, revealing constant mixing ratios with values of 30–35 ppb and 70–80 ppb for O_3 and CO, respectively.

Under these conditions, could be observed the O_3, CO and NO_2 background values in this region.

To investigate the spatial distribution of O_3, CO and NO_2, the CAMS model output was used (Fig. 2c-d-e). Under westerly flows, the CO fields showed lower mixing ratios in marine regions than in continental regions. The lower CO mixing ratios were clearly observed in areas where the wind blows intensely, and increases when the dispersion decreases, such as in southern South America. In this last case, CO could be accumulated in the lower layers and be associated with the continental emissions.

Although the evaluation of the CAMS model is not the aim of this work, there was a clear underestimation of the CO values (~35–40 ppb) obtained with the model, with respect to the experimental observations (~60 ppb). A similar behavior was obtained for NO_2, although, in this case, the mixing ratios were low in a large area of the studied region. Therefore, an increase of CO and NO_2 was identified, attributed to a weak horizontal dispersion in regions located north of 52 ^{0}S latitude. However, O_3 showed a horizontal distribution opposite to that of CO and NO_2, with high and low mixing ratios in marine and continental areas, respectively. As expected, O_3 in the continental area undergoes elimination processes: both chemical elimination, associated with anthropogenic emissions, and dry deposition. This O_3 decrease was clearly observed at the Ushuaia region in the maps of January 18th 2016 (Fig. 2c); in this case, the values computed by the model were similar to the experimental observations.
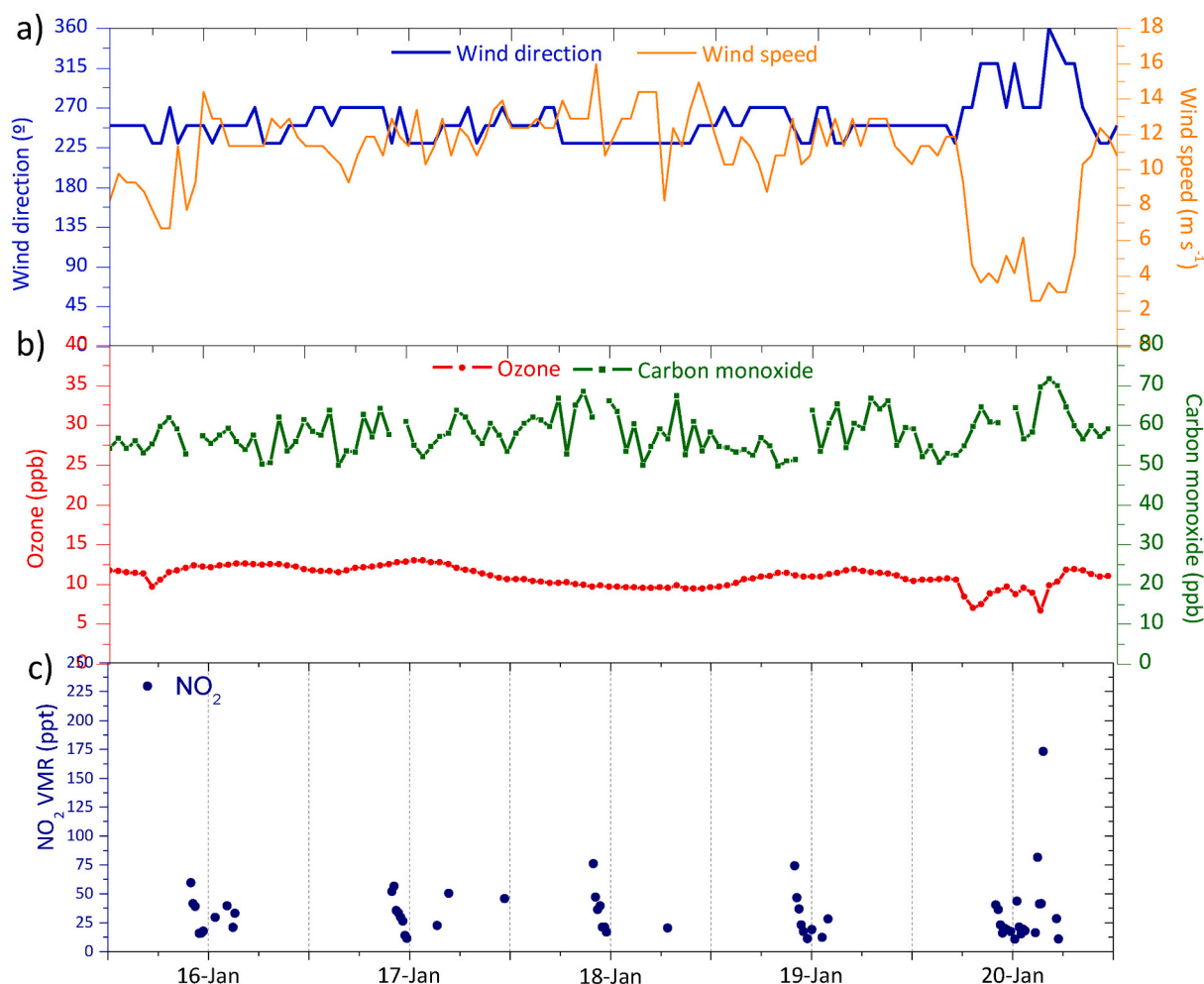

Fig. 3. Temporal evolution for January 16th–20th 2016 for wind (direction and speed) (a), O_3 and CO (b) and NO_2 volume mixing ratios (VMR) (c).

3.3. Impact of the local scale on O_3, CO and NO_2

A pattern characterized by a decrease of O_3 and a rise of CO and NO_2 was observed during specific periods. Applying the criteria mentioned in Section 2.5, the periods with this behavior were identified. On the one hand, it was obtained that an event with at least two hours of duration occurred in $45.8 \pm 3.4\%$ of the days, oscillating between 50.8% in 2013 and 41.8% in 2018. No trends in this percentage of occurrence were observed. The duration of the events ranged between 2 and 7 h. Events with different duration in hours during the same day, and even on consecutive days, were obtained. On the other hand, as expected, it was observed that the longest events, longer than 5 h, occurred mostly in the coldest months, between May and September, since the winter months are distinguished by thermal inversions or weak development of the mixing layer, thus favoring the accumulation of emissions in the lower layers. In addition, the annual number of hours with events was accounted, obtaining an average annual frequency of $6.4 \pm 0.5\%$, ranging between 6.6% (in 2011 and 2016) and 7.9% (2013). As expected, taking into account the small number of days showing this behavior, no trend was observed with the frequency in hours. For example, in 2013, this was only observed 50.8% of days with events, with a total of 648 h, i.e., an annual frequency of 7.9%.

The occurrence of this pattern is associated with a decrease in the wind speed, since an average of 2.1 ± 1.3 m s^{-1} was obtained for the identified events, which corresponds to almost atmospheric stagnation. An analysis of O_3 and CO mixing ratios, in these events, revealed an O_3 mean of 11.0 ± 5.8 ppb; therefore, the O_3 destruction was around 45% (taking as reference the annual mean of 20.3 ± 7.6 ppb). While the accumulation of CO close to the ground showed a mean of 161.1 ± 83.2 ppb, the annual average of the CO peaks in these events was usually 567.1 ± 101.1 ppb.

Several events were analyzed in detail. However, to explore the origin of this pattern and determine representative values of duration and recorded mixing ratios, the period of July 2nd-10th 2018 was selected. To investigate the weather conditions under which these patterns occurred, MSLP and wind fields obtained from the ERA5 data reanalysis were used (Fig. 4). It was observed that this pattern is given under weather conditions governed by a high-pressure system, which affects the study region, causing a decrease in horizontal advection or even atmospheric stagnation.

The high-pressure system, which ends up influencing the study region, can evolve in three different ways: i) movement of the high-pressure system located in the south of the Pacific Ocean towards lower latitudes and positioning in the western part off the coasts of
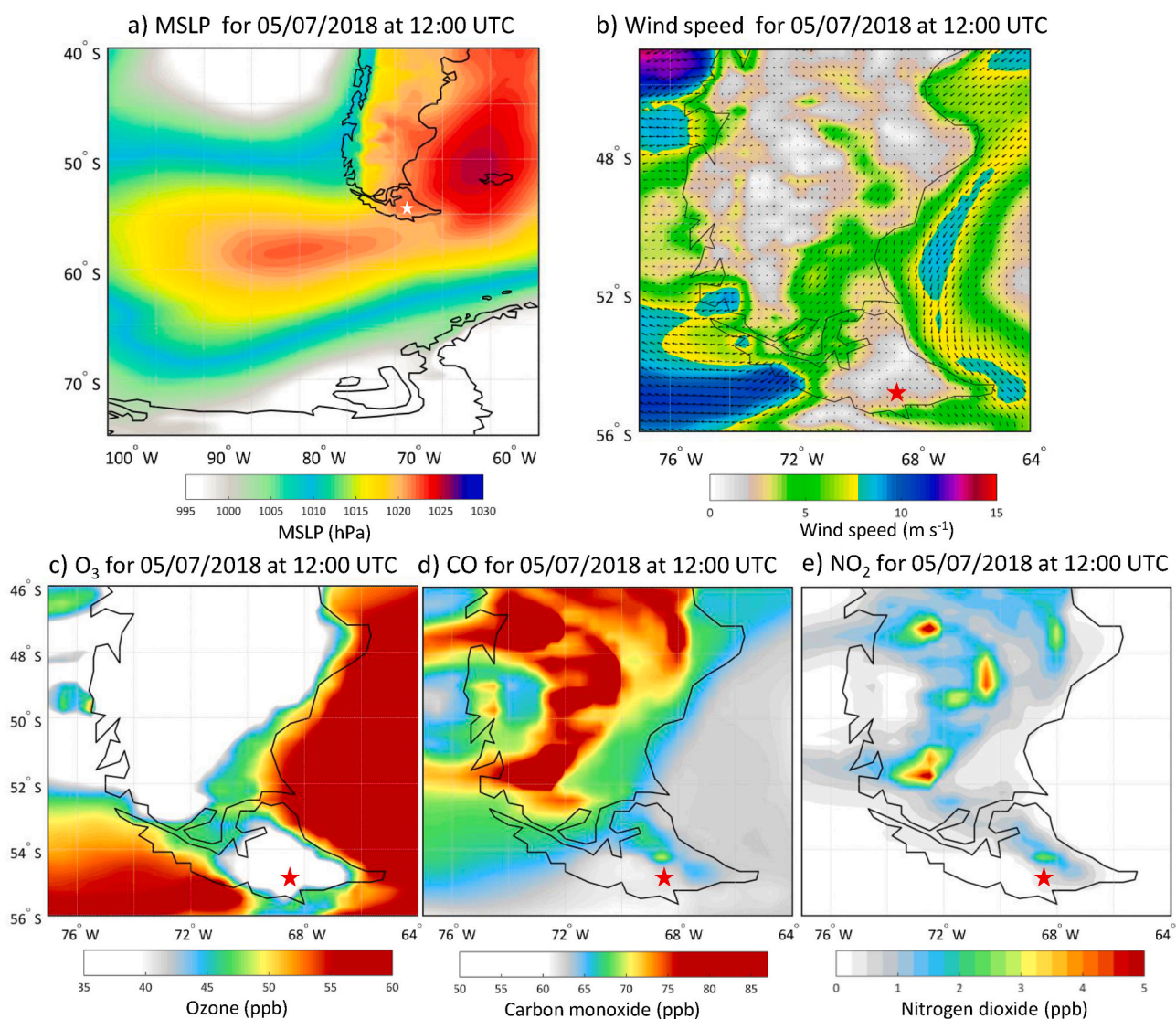
Fig. 4. Mean sea level pressure (MSLP) and wind fields for July 5th 2018 at 12:00 UTC (a-b), and CO, O_3 and NO_2 spatial distribution obtained from the CAMS model with a $0.25^0 \times 0.25^0$ spatial resolution (c-d-e). Location of Ushuaia (star).

South America; ii) high-pressure system located in the continental region of South America and going towards lower latitudes, which, in some occasions, may not only affect the Ushuaia region, but also the west side of Drake Passage (this is what happened in the event of July 2018, see Fig. 4a); and iii) high-pressure system located in the south of the Atlantic Ocean, moving southwards and affecting the southern part of South America. With these isobaric configurations, the impact at the Ushuaia region is the same: the high-pressure system blocks the low-pressure system located in lower latitudes and close to the continent of Antarctica, inhibiting western airflows, which causes the wind speed to decrease or even reached atmospheric stagnation at the Ushuaia region, as occurred on July 5th 2018 (Fig. 4b). The usual conditions return, i.e., westerly airflows, with the weakening of the high-pressure system and the displacement of the low-pressure system to the north.

In the selected event of July 2018, there was wind blowing from the west with a wind speed of 12–14 m s^{-1}. Due to the influence of the high-pressure system, the westerly winds were blocked and, in the early hours of July 3rd 2018, an abrupt decrease in the wind speed was recorded, with hourly values below 2–3 m s^{-1}. Onwards, the wind direction showed mainly a north component, oscillating with wind speeds between ~2 and 4 m s^{-1} and even calm winds. These conditions remained until noon on July 8th 2018, when the low-pressure system returned to its usual position and the westerlies started to blow with wind speed higher than 6–8 ms^{-1}, typical values in these conditions. (Fig. 5a).

The evolution of the experimental temperature and the ABL height obtained from ERA5 were explored in this particular period (Fig. 5b). A strong correlation was observed between wind speed, temperature and ABL height.

As was previously mentioned, under anticyclonic conditions, there was a decrease of wind speed associated with a decrease of temperature. The daily mean temperature on July 6th and 8th 2018 was −1.0 ± 1.6 °C and 8.6 ± 2.1 °C, respectively. Likewise, there was a decrease in ABL height, which barely reached 100 m under these conditions, while the maximum ABL height was up to 800–1000 m under a scenario governed by westerly flows, as occurred on July 2nd and 9th before and after the event, respectively.

Atmospheric stagnation promotes a further cooling of the ground and a greater thermal vertical stability. Otherwise, when the air blows from the Pacific Ocean, this marine air mass is warmer and favors the development of the ABL.

As is known, the meteorological conditions have a direct impact on the behavior of the studied trace gases. Before such event, on July 2nd and 3rd 2018, mixing ratios (both during the day and at night time) of ~30–35 ppb and ~ 55–60 ppb were registered for O_3 and CO, respectively, while the measured NO_2 values remained below the detection limit (about 5 ppt for this particular day) (Fig. 6ab).

The decrease in the wind speed simultaneously caused a sharp drop in the O_3 mixing ratios, along with an unexpected increase of CO and NO_2. On July 4th 2018 at 6:00 UTC, 55 ppb of CO and 32 ppb of O_3 were measured. However, 12 h later, at 18:00 UTC, 340 ppb of CO, 12 ppb of O_3 and up to 2200 ppt of NO_2 were registered (Fig. 6).

Therefore, the mixing ratio of CO was multiplied by a factor of 6, NO_2 by more than 10 and O_3 decreased by a factor of approximately 4.5. On these days, CO peaks higher than 440 ppb were observed on July 4th at 12:00 UTC, July 5th at 18:00 UTC and July 8th at 1:00 UTC. These were elevated and unexpected CO values for a background environment such as Ushuaia, whereas NO_2 showed peaks higher than 3000 ppt on July 4th–8th 2018, with a maximum of 3700 ppt registered on July 6th 2018. The weak or null advection favored the accumulation of the chemical species emitted by local sources in the lower atmospheric layers. The photochemical O_3 removal was probably driven by the CO and NO_x emissions, depressed through a phenomenon defined as NO_x titration ($NO+O_3 \rightarrow NO_2 + O_2$), although other destruction processes, such as the removal with HO_x radicals, could not be discarded.

This observed pattern at Ushuaia occurred at the regional level. The O_3, CO and NO_2 fields obtained with the CAMS model (Fig. 4c to e) showed an increase of CO and NO_2 both in the Tierra del Fuego region and in areas further north (July 5th 2018) and low O_3 mixing ratios in a specific area of Ushuaia and Tierra del Fuego. On July 9th 2018 onwards, the weather conditions changed, and an increase in the horizontal dispersion, associated with the west airflows, caused a decrease in the CO and NO_2, with the recovery of ozone values.

The NO_2 MAXDOAS measurement allows the retrieval of profiles (section 2.3). Fig. 6c shows the NO_2 profile in this event of July 2018.
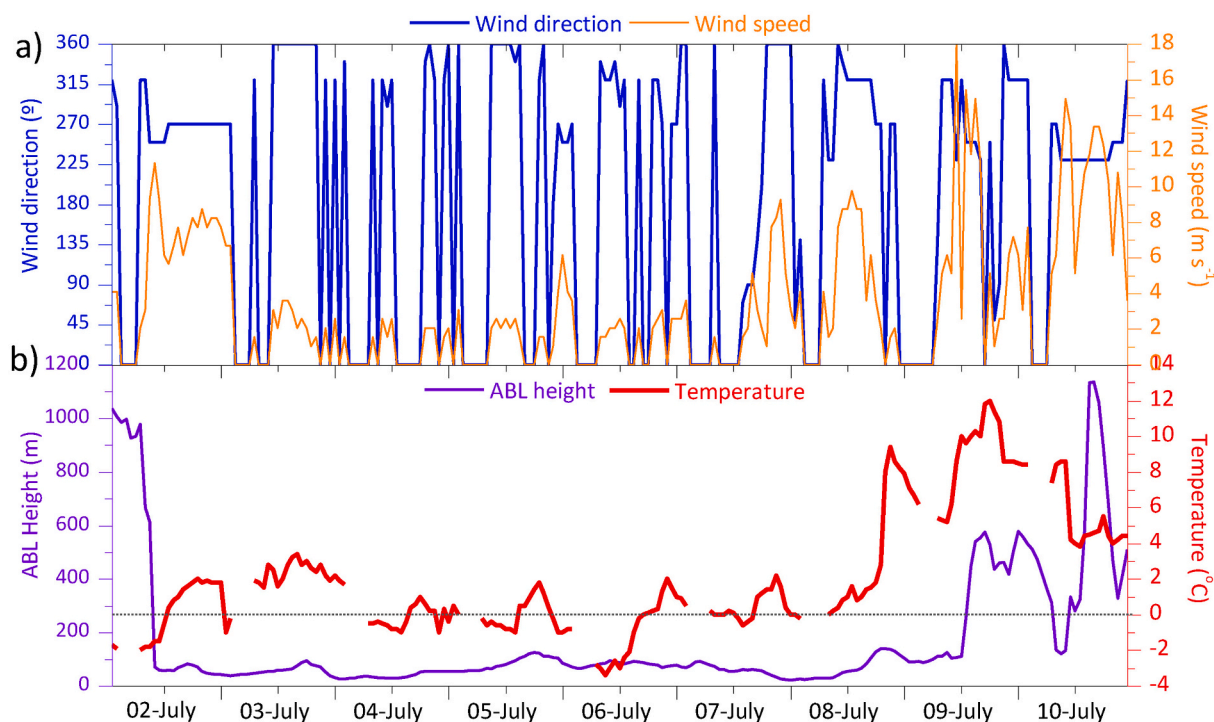

Fig. 5. Temporal evolution for July 2nd-10th 2018 for wind (direction and speed) (a), atmospheric boundary layer (ABL) height from ERA5 and temperature (b).
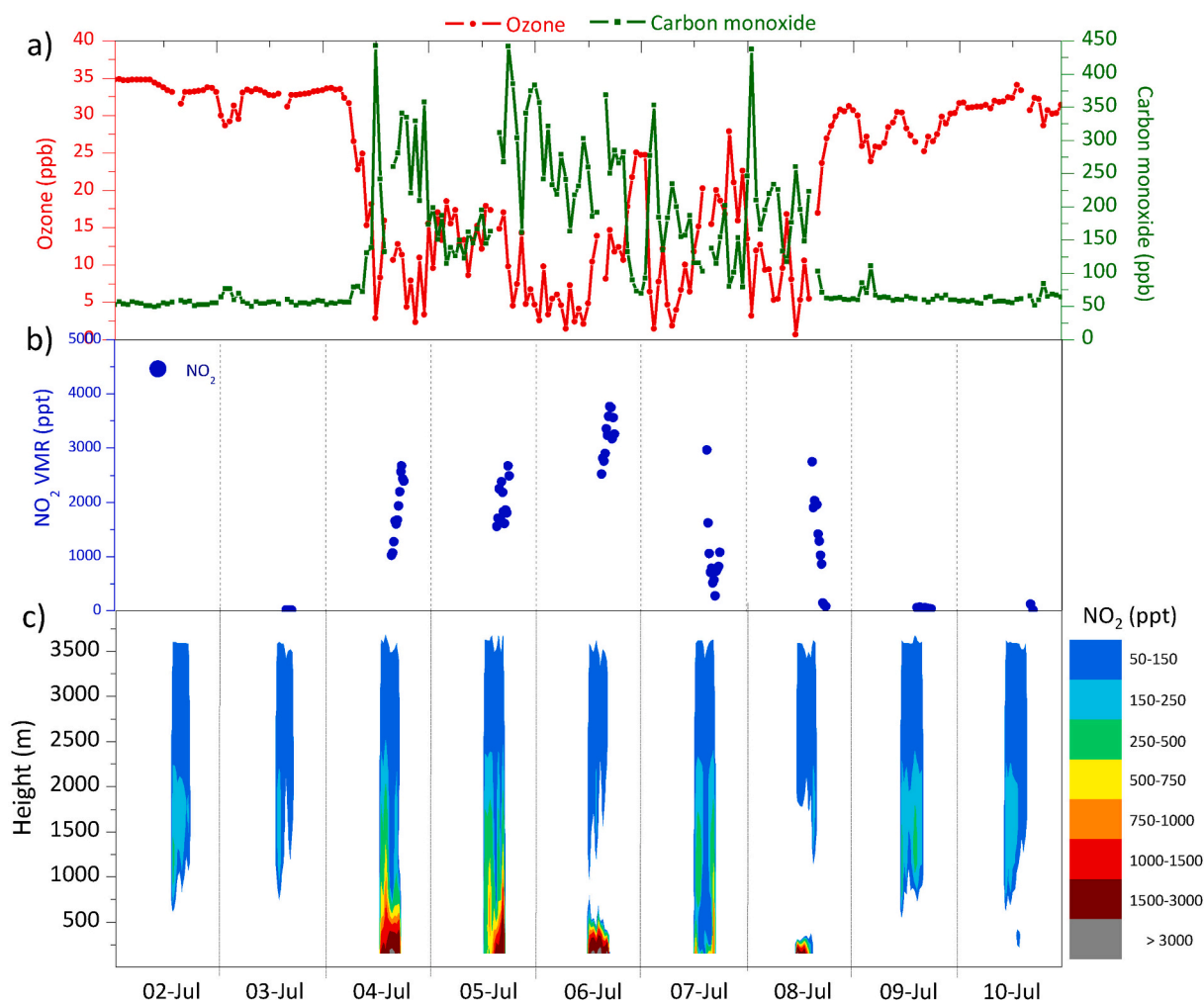
Fig. 6. Temporal evolution for July 2nd-10th 2018 for CO and O_3 (a), NO_2 volume mixing ratios (VMR) (b) and retrieved NO_2 profile (c).

Prior to the event, on July 2nd and 3rd, NO_2 was below detection limit of 10 ppt in the first kilometers, thus, with westerly winds and wind speeds higher than 8 m s^{-1}, the atmospheric ventilation not only occurred on the surface but also in at least the first three kilometers. The ABL development these days reached a maximum height of ~800 m. During the event, in July 4th–8th 2018, clearly NO_2 was observed in the upper layers.

The event started on July 4th and 5th, when a NO_2 distribution in the first kilometer and a maximum ABL height of ~50–70 m were observed. The highest NO_2 mixing ratios were obtained in the first 500 m (up to 4500 ppts), while above 500 m there were mixing ratios of up to ~2000 ppts. On July 6th, NO_2 was accumulated in the first hundreds of meters, i.e., within the first kilometer. The levels of NO_2 close to the ground were the highest of this event, which was expected, since less development of the ABL associated with temperature below 0 °C favored the accumulation of NO_2 on the surface. The event finished with an increase in wind speed, temperature and maximum ABL height. A major vertical and horizontal dispersion resulted in low values of NO_2 or event close to zero.

Whether it is assumed that the NO_2 vertical behavior obtained is similar to other chemical species such as CO, the occurrence of westerly flows or atmospheric stagnation determines the horizontal wind speed, temperature and the development of the ABL, as well as the behavior of the trace gases.

3.4. Annual temporal evolution of O_3 and CO: Unexpected positive CO trend

Despite the short data series available (11 years), the variation of O_3 and CO in the last decade was explored using the annual averages. Fig. 7a shows the annual temporal evolution of O_3 and CO at Ushuaia and their linear fits. An annual anticorrelation between O_3 and CO was observed, i.e., an increase of CO vs a decrease of O_3 and vice versa.

The annual values of O_3 oscillated between 19.0 ± 5.3 ppb in 2016 and 22.0 ± 4.3 ppb in 2018, with an annual amplitude of ~3 ppb in such period. O_3 showed interannual variations: the first 3 years (2010−2012) showed an upward trend, and in the following years, until 2016, the annual values decreased. In the last three years (2016–2018), the trend started to increase again. Using the linear fit of O_3 in the whole period, a slope of 0.07 ± 0.12 ppb year^{-1} ($r = 0.24$ and $\rho = 0.53$) was obtained; i. e., no significant trend was found. Similar result was found in Cape Grim (Tasmania, Australia) with a trend of 0.06 ± 0.02 ppb year^{-1} ($r = 0.71$) using the period 1982–2010 (Cooper et al., 2014) and El Tololo (Chile) with 0.67 ppb decade^{-1} ($\rho = 0.63$) from 1995 to 2010 (Anet et al., 2017; Cooper et al., 2020). However, the trend of Ushuaia was slightly lower to obtained for Cape Point (South Africa) with a trend of 0.19 ± 0.05 ppb year^{-1} ($r = 0.85$) in the interval from 1983 to 2011 (Cooper et al., 2014).

The yearly averages of CO vary between 59.3 ± 15.0 ppb in 2010 and 79.0 ± 1 9.5 ppb in 2017, with an annual amplitude of ~20 ppb. In contrast to the result obtained for O_3, CO showed a positive trend with a slope of 1.75 ± 0.49 ppb year^{-1} ($r = 0.80$ and $\rho = 0.09$), i.e an annual increase of 1.6 ppb year^{-1}. Therefore, in the last decade, the CO mixing
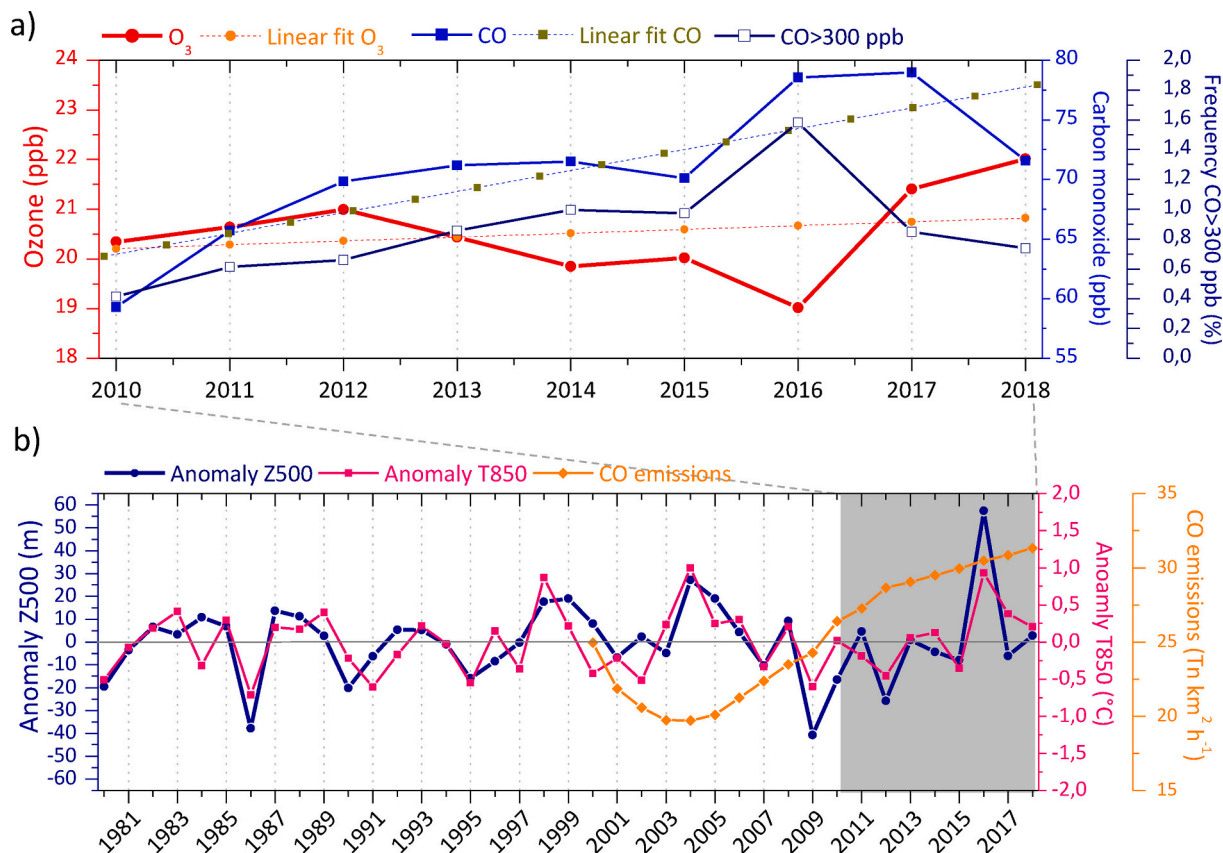
Fig. 7. Ozone and carbon monoxide annual temporal evolution and their linear fits, annual frequency of hours with hourly CO values higher than 300 ppb (a) in the period of 2010–2018, annual temporal evolution of the anomalies for the geopotential height at 500 hPa (Z500) and temperature at 850 hPa (T850) from ERA5 data reanalysis between 1980 and 2018 and CO emissions at the Ushuaia area (b). The reference period for the climatological series was 1981–2010.

ratios increased by ~22%. The trend observed in Ushuaia was opposite to others CO trends obtained in the southern hemisphere. Thus, for example in Wollongong (Australia) was obtained a short-term trends of -11 ppb year^{-1} using in situ observations in the period 2011 to 2014 (Buchholz et al., 2016); in Lauder, (New Zealand) was registered a decrease of $0.94 \pm 0.47\%$ yr^{-1} in CO columns measured with a FTIR (Fourier Transform Spectroscopy) instrument during the period 1997–2009 (Zeng et al., 2012); while using observations from four instruments onboard satellites, was detected a decrease in the Southern Hemisphere (0–60°) oscillating between 0.54 ± 0.44 (period 2003–2011) and 2.4 ± 2.7 (period 2005–2009) in % yr^{-1} (Worden et al., 2013).

To determine whether this increase could be attributed in the whole range of CO values, the annual frequency of occurrence of the number of hours with CO mixing ratios higher than 300 ppb (Fig. 7a) was analyzed. The obtained results point out that the variation in the annual number of these events strongly influences the annual averages variation. Therefore, the CO annual average is increasing due to the increase in CO peaks, registered under anticyclonic conditions with almost atmospheric stagnation (Section 3.3). The explanation of this upward trend in the annual CO should be associated with changes in the emissions, changes in the weather conditions or both simultaneously.

In order to explore whether this fact was associated with the weather conditions, the annual anomalies of temperature (T850) and geopotential height (Z500) were analyzed in the 850 and 500 hPa levels, respectively. The monthly values from the ERA5 data reanalysis were obtained for Ushuaia, and then the annual averages were obtained from these values. According to the definition of the World Meteorological Organization (WMO 2017a), to identify climatological changes, a recent 30-year period must be investigated, since it is most representative of

normal conditions. The 1981–2010 baseline period is used, at present, for climate monitoring (WMO, 2019). To investigate whether the possible changes in the meteorological conditions only occurred in the last decade or in a longer period, such a climatological reference period was taken into consideration. Currently, ERA5 has available datasets from 1979 to present. Therefore, the annual anomalies for the temperature and geopotential heights were calculated from 1981 to 2018 (Fig. 7b).

As was expected, a clear correlation was obtained in the anomalies of T850 and Z500. In the 80s and 90s, a typical year-on-year variation is observed, with the anomalies oscillating around zero; it is worth highlighting the negative anomalies of 1986 and the positive anomalies of 1998–1999. In the 2000s, the first eight years were dominated by positive anomalies, and, from 2009, the anomalies were mainly negative, exception for 2016, which presented the maximum positive anomaly for the historical series of almost the last 40 years.

Positive temperature and geopotential height anomalies at 850 hPa and 500 hPa levels are an indicator of anticyclonic conditions, which would induce a local surface high-pressure system that promotes weak airflows or atmospheric stagnation (Horton et al., 2016). In the last decade, there was no clear positive trend in T850 or Z500 anomalies, which would result in a greater number of atmospheric stagnation situations and an increase of CO mixing ratios. This result was in agreement with the identification of the pattern governed by the local scale (Section 3.3.), which did not show any trend in the last decade, with a similar frequency of occurrence throughout the whole period. Therefore, it can be assumed that the upward CO trend could not be attributed to a change in the weather conditions.

Emissions are the second factor that could be affecting CO mixing ratios. To explore it, the annual evolutions provided by the Copernicus

emissions inventory were used, applying an area-average of 1° x 1° around Ushuaia (Fig. 7b). Since the inventory provides information since 2000, we can see if the changes were recent or prior to this date. Although in the Fig. 7b are shown the total emissions, an annual analysis of them, according to the source sector, showed to the traffic as the main CO source with an $84.7 \pm 1.8\%$ followed by the domestic heating with a $9.9 \pm 1.4\%$ in the period 2000–2018.

The 2000s began with a clear decline in CO emissions: an annual 5% decrease between 2000 and 2004. These years coincide with a strong economic crisis in Argentina, which began in the late 1990s. Accordingly, the CO decrease could be attributed to a slowdown in human activity due to the economic crisis. From 2005 onward, the economic activity activation could be the factor that led to a change in CO trends, since a clear upward trend in the CO emissions at Ushuaia was observed in the emission inventories. In the last 13 years (2005–2018), an increment of 4.4% per year (absolute increase of 58%) was obtained in CO emissions, from 20.1 Tn km^2 h^{-1} in 2005 to 31.1 Tn km^2 h^{-1} in 2018. However, in the last nine years, this positive trend decreased, with a yearly variation of 2.1%. Therefore, the results were similar, i.e., an increment of annual CO mixing ratio of 22% and an increase of CO emissions of 19% in the same period. Thus, it is evident that the observed CO upward trend can be attributed to an increase of emissions.

As was previously mentioned, the highest CO mixing ratio occurs under anticyclonic conditions, and even if their frequency did not change, the higher the emissions, the higher the registered CO concentrations are.

As could be expected in a warm climate, if the meteorological conditions change through a greater number of anticyclonic situations, with positive anomalies of T850 and Z500, both factors, i.e., emissions and meteorology, could contribute to this CO increase. In that case, the levels of not only CO but probably other chemical species, such as NO_2, would be expected to undergo a considerable increase. Such a situation took place in the year 2016, with clearly increasing emissions and with the highest positive anomalies of T850 and Z500 of almost the last four decades. This resulted in the second highest annual CO value of the whole studied period, with 78.5 ± 17.9 ppb, a difference of 0.5 ppb and an annual mean of 79.0 ± 19.5 ppb for 2017. 2016 is also the year presenting the largest number of hours, with CO mixing ratios higher than 300 ppb.

If in the next years or decades, emissions continue to increase and the weather conditions are similar to those of 2016 or show even higher positive anomalies, a substantial change in the atmospheric composition of this region could be expected, which would have unknown implications.

4. Conclusions

In this work, we explored the behavior patterns of two trace gases, i. e., ozone (O_3) and carbon monoxide (CO), at the GAW-WMO (Global Atmospheric Watch – World Meteorological Organization) station of Ushuaia (Argentina). The hourly mixing ratios measured for nine years (2010–2018) were used.

An overview of the data series showed a 95th percentile of 32.1 ppb and 164.5 ppb for O_3 and CO, respectively. While the absolute maximum values were 40 ppb for O_3 measured on June 2010 and 735 ppb for CO recorded on May 26th 2015, the mean and median values were 20.3 ± 7.6 ppb and 19.8 ppb for O_3 and 72.9 ± 47.5 ppb and 59.6 ppb for CO, respectively. To investigate the emissions affecting this region, the emission inventory of Copernicus was used, taking CO as tracer. The main sources were identified at the Ushuaia region itself, as well as in regions located in the north.

Based on previous studies, two behavior patterns for O_3 and CO were identified. Representative periods of each pattern were analyzed in detail. Furthermore, in these events, NO_2 measurements obtained with a MAXDOAS instrument were also analyzed.

The most frequent pattern is characterized by O_3 and CO mixing

ratios that remained unchanged for days, with values of 10–15 ppb and 60–70 ppb, respectively, and below 200 ppt for NO_2. This pattern is associated with weather conditions governed by the intense westerly airflows caused by a low-pressure system located in the south of the Pacific Ocean. The O_3, CO and NO_2 horizontal distributions obtained from the CAMS model suggest that not only the Ushuaia observatory but a large region situated in the south of South America showed the same behavior, i.e., low CO mixing ratios, almost null values of NO_2 and low O_3 values in continental areas, while the surrounding marine areas showed higher mixing ratios.

Applying a specific criterion, events with a second type of pattern were identified. In $45.8 \pm 3.4\%$ of the days, an event of at least two hours occurred. The total number of hours with an event was 26, which translates into an average annual frequency of $6.4 \pm 0.5\%$. This pattern is characterized by low O_3 mixing ratios (~12 ppb), elevated NO_2 values (higher than ~3000 ppt) and CO values with peaks exceeding 400 ppb. This scenario was caused by the influence of a high-pressure system, which blocked the westerly winds and caused atmospheric stagnation. The winter months favor the temperature decrease, strong vertical stability and an almost null ABL development, with the subsequent accumulation of trace gases such as CO and NO_2 in the lower troposphere.

The annual trend of O_3 and CO was explored. While no O_3 trend was obtained, in the case of CO, an unexpected upward trend was identified, with an increase of 1.75 ± 0.49 ppb year^{-1} (22% in the whole period of nine years). To investigate its causes, both meteorological and emissions factors were analyzed. Possible changes in the weather conditions were studied along with the annual variation of the temperature anomalies (T850) and geopotential height (Z500), obtaining no trends. Annual CO emissions showed an increasing trend of 2.1% per year (19% in the whole period); therefore, the CO increase could be attributed to the emission changes. Since the traffic is the main source of CO in this area (~85%), this increase could be attributed to the increase of the traffic, which could be associated with a growth of the city.

In remote regions such as Ushuaia, future studies should be conducted to identify possible changes in the weather patterns and in the levels of trace gases, since, in a future warm climate governed by more anticyclonic situations, along with a growing trend in emissions, an outstanding change in the atmospheric composition could occur.

Declaration of Competing Interest

The authors declare that they have no known competing financial interests or personal relationships that could have appeared to influence the work reported in this paper.

References

Adame, J.A., Cupeiro, M., Yela, M., Cuevas, E., Carbajal, G., 2019. Ozone and carbon monoxide at the Ushuaia GAW-WMO global station. Atmos. Res. 217, 1–9. https://doi.org/10.1016/j.atmosres.2018.10.015.

Anderson, G.P., Clough, S.A., Kneizys, F.X., Chetwynd, J.H., Shettle, E.P., 1986. AFGL Atmospheric Constituent Profiles (0–120 km), Tech. Rep., AFGL-TR-86-0110, Env. Res. Papers, No. 954.

Anet, J.G., Steinbacher, M., Gallardo Klenner, L., Velásquez Álvarez, P.A., Emmenegger, L., Buchmann, B., 2017. Surface ozone in the Southern Hemisphere: 20 years of data from a site with a unique setting in El Tololo, Chile. Atmos. Chem. Phys. 17, 6477–6492.

Buchholz, R.R., Paton-Walsh, C., Griffith, D.W., Kubistin, D., Caldow, C., Fisher, J.A., Deutscher, N.M., Kettlewell, G., Riggenbach, M., Macatangay, R., Krummel, P.B., Langenfelds, R.L., 2016. Source and meteorological influences on air quality (CO, CH_4 and CO_2) at a Southern Hemisphere urban site. Atmos. Environ. 126, 274–289.

C3S, 2017. ERA5: Fifth generation of ECMWF atmospheric reanalyses of the global climate. In: Copernicus Climate Change Service Climate Data Store (CDS). https://cds.climate.copernicus.eu/cdsapp#!/home.

Clémer, K., Van Roozendael, M., Fayt, C., Hendrick, F., Hermans, C., Pinardi, G., Spurr, R., Wang, P., De Mazière, M., 2010. Multiple wavelength retrieval of tropospheric aerosol optical properties from MAXDOAS measurements in Beijing. Atmos. Meas. Tech. 3, 863–878.

Cooper, O.R., Parrish, D.D., Ziemke, J., Balashov, N.V., Cupeiro, M., Galbally, I.E., Gilge, S., Horowitz, L., Jensen, N.R., Lamarque, J.-F., Naik, V., Oltmans, S.J., Schwab, J., Shindell, D.T., Thompson, A.M., Thouret, V., Wang, Y., Zbinden, R.M., 2014. Global distribution and trends of tropospheric ozone: an observation-based review. Elem. Sci. Anthrop. 2, 000029.

Cooper, O.R., Schultz, M.G., Schröder, S., Chang, K.-L., Gaudel, A., Carbajal, G., Cuevas, E., Fröhlich, M., Galbally, I.E., Molloy, S., Kubistin, D., Lu, X., McClure-Begley, A., Nédélec, P., O'Brien, J., Oltmans, S.J., Petropavlovskikh, I., Ries, L., Senik, I., Sjöberg, K., Solberg, S., Spain, G.T., Spang, W., Steinbacher, M., Tarasick, D., Thouret, V., Xu, X., 2020. Multi-decadal surface ozone trends at globally distributed remote locations. Elem. Sci. Anthrop. 8, 23.

Coumou, D., Di Capua, G., Vavrus, S., Wang, L., Wang, S., 2018. The influence of Arctic amplification on mid-latitude summer circulation. Nat. Commun. 9 (1), 1–12.

Crippa, M., Guizzardi, D., Muntean, M., Schaaf, E., Dentener, F., van Aardenne, J.A., Monni, S., Doering, U., Olivier, J.G.J., Pagliari, V., Janssens-Maenhout, G., 2018. Gridded emissions of air pollutants for the period 1970–2012 within EDGAR v4.3.2. Earth Syst. Sci. Data 10, 1987–2013.

Dominé, F., Albert, M., Huthwelker, T., Jacobi, H.-W., Kokhanovsky, A.A., Lehning, M., Picard, G., Simpson, W.R., 2008. Snow physics as relevant to snow photochemistry. Atmos. Chem. Phys. 8, 171–208.

ECMWF, 2017. IFS documentation - Cy43r3. Operational Implementation. Part IV: Physical Processes (221 pp).

Flannigan, M., Stocks, B., Turetsky, M., Wotton, M., 2009. Impacts of climate change on fire activity and fire management in the circumboreal forest. Glob. Chang. Biol. 15, 549–560.

Gomez, L., Navarro-Comas, M., Puentedura, O., Gonzalez, Y., Cuevas, E., Gil-Ojeda, M., 2014. Long-path averaged mixing ratios of O_3 and NO_2 in the free troposphere from mountain MAX-DOAS. Atmos. Meas. Tech. 7, 3373–3386.

Granier, C., Darras, S., van der Denier Gon, H., Doubalova, J., Elguindi, N., Galle, B., Gauss, M., Guevara, M., Jalkanen, J., Kuenen, J., Liousse, C., Quack, B., Simpson, D., Sindelarova, K., 2019. The Copernicus Atmosphere Monitoring Service global and regional emissions (April 2019 version), Copernicus Atmosphere Monitoring Service (CAMS) report, 2019. https://doi.org/10.24380/d0bn-kx16.

Hersbach, H., Dee, D., 2016. ERA5 reanalysis is in production. ECMWF Newslett. 7.

Hoesly, R.M., Smith, S.J., Feng, L., Klimont, Z., Janssens-Maenhout, G., Pitkanen, T., Seibert, J.J., Vu, L., Andres, R.J., Bolt, R.M., Bond, T.C., Dawidowski, L., Kholod, N., Kurokawa, J.-I., Li, M., Liu, L., Lu, Z., Moura, M.C.P., O'Rourke, P.R., Zhang, Q., 2018. Historical (1750–2014) anthropogenic emissions of reactive gases and aerosols from the Community Emissions Data System (CEDS). Geosci. Model Dev. 11 (369–408), 2018. https://doi.org/10.5194/gmd-11-369-2018.

Horton, R.M., Mankin, J.S., Lesk, C., Coffel, E., Raymond, C., 2016. A review of recent advances in research on extreme heat events. Curr. Clim. Change Rep. 2, 242–259.

Huijnen, V., Eskes, H.J., Wagner, A., Schulz, M., Christophe, Y., Ramonet, M., 2016. Validation Report of the CAMS Near-Real-Time Global Atmospheric Composition Service: System Evolution and Performance Statistics. Status up to 1 June 2016.

Kang, H., Zhu, B., Zhu, C., van der Ronald, A.J., Zhu, C., de Leeuw, G., Hou, X., Gao, J., 2019. Natural and anthropogenic contributions to long-term variations of SO_2, NO_2, CO, and AOD over East China. Atmos. Res. 215, 284–293.

Li, K., Jacob, D.J., Liao, H., Shen, L., Zhang, Q., Bates, K.H., 2019. Anthropogenic drivers of 2013–2017 trends in summer surface ozone in China. Proc. Natl. Acad. Sci. 116 (2), 422–427.

Magee, J., 2016. Climate change in deserts: past, present and future. Quat. Australas. 33 (1), 34–35.

Monks, P.S., Archibald, A.T., Colette, A., Cooper, O., Coyle, M., Derwent, R., Fowler, D., Granier, C., Law, K.S., Mills, G.E., Stevenson, D.S., Tarasova, O., Thouret, V., von Schneidemesser, E., Sommariva, R., Wild, O., Williams, M.L., 2015. Tropospheric ozone and its precursors from the urban to the global scale from air quality to short-lived climate forcer. Atmos. Chem. Phys. 15, 8889–8973.

Parrish, D.D., Galbally, I.E., Lamarque, J.F., Naik, V., Horowitz, L., Shindell, D.T., Oltmans, S.J., Derwent, R., Tanimoto, H., Labuschagne, C., Cupeiro, M., 2016. Seasonal cycles of O3 in the marine boundary layer: Observation and model simulation comparisons. J. Geophys. Res.-Atmos. 121 (1), 538–557.

Peters, E., Pinardi, G., Seyler, A., Richter, A., Wittrock, F., Bösch, T., Van Roozendael, M., Hendrick, F., Drosoglou, T., Bais, A.F., Kanaya, Y., Zhao, X., Strong, K., Lampel, J., Volkamer, R., Koenig, T., Ortega, I., Puentedura, O., Navarro-Comas, M., Gómez, L., Yela González, M., Piters, A., Remmers, J., Wang, Y., Wagner, T., Wang, S., Saiz-Lopez, A., García-Nieto, D., Cuevas, C.A., Benavent, N., Querel, R., Johnston, P., Postylyakov, O., Borovski, A., Elokhov, A., Bruchkouski, I., Liu, H., Liu, C., Hong, Q., Rivera, C., Grutter, M., Stremme, W., Khokhar, M.F., Khayyam, J., Burrows, J.P., 2017. Investigating differences in DOAS retrieval codes using MAD-CAT campaign data. Atmos. Meas. Tech. 10, 955–978.

Pires, J.C.M., Alvim-Ferraz, M.C.M., Martins, F.G., 2012. Surface ozone behaviour at rural sites in Portugal. Atmos. Res. 104, 164–171.

Platt, U., Stutz, J., 2008. Differential Optical Absorption Spectroscopy: Principles and Applications, Springer Verlag, 2008.

Prados-Roman, C., Gómez-Martín, L., Puentedura, O., Navarro-Comas, M., Iglesias, J., De Mingo, J.R., Pérez, M., Ochoa, H., Barlasina, M.E., Carbajal, G., Yela, M., 2018. Reactive bromine in the low troposphere of Antarctica: estimations at two research sites. Atmos. Chem. Phys. 18, 8549–8570.

Rodgers, C., 2000. Inverse Methods for Atmospheric Sounding, World Scientific, Singapore, New Jersey, London, Hongkong, 2000.

Roesch, A., Wild, M., Pinker, R., Ohmura, A., 2002. Comparison of spectral surface albedos and their impact on the general circulation model simulated surface climate. J. Geophys. Res. 107 (D14), 4221.

Seguel, R.J., Gallardo, L., Fleming, Z.L., Landeros, S., 2020. Two decades of ozone standard exceedances in Santiago de Chile. Air Qual. Atmos. Health 1–13.

Spurr, R., 2008. LIDORT and VLIDORT: linearized pseudo-spherical scalar and vector discrete ordinate radiative transfer models for use in remote sensing retrieval problems. In: Kokhanovsky, A. (Ed.), Light Scattering Reviews 3, Springer Praxis Books, 7. Springer, Berlin Heidelberg, pp. 229–275.

Tirpitz, J.-L., Frieß, U., Hendrick, F., Alberti, C., Allaart, M., Apituley, A., Bais, A., Beirle, S., Berkhout, S., Bognar, K., Bösch, T., Bruchkouski, I., Cede, A., Chan, K.L., den Hoed, M., Donner, S., Drosoglou, T., Fayt, C., Friedrich, M.M., Frumau, A., Gast, L., Gielen, C., Gomez-Martín, L., Hao, N., Hensen, A., Henzing, B., Hermans, C., Jin, J., Kreher, K., Kuhn, J., Lampel, J., Li, A., Liu, C., Liu, H., Ma, J., Merlaud, A., Peters, E., Pinardi, G., Piters, A., Platt, U., Puentedura, O., Richter, A., Schmitt, S., Spinei, E., Stein Zweers, D., Strong, K., Swart, D., Tack, F., Tiefengraber, M., van der Hoff, R., van Roozendael, M., Vlemmix, T., Vonk, J., Wagner, T., Wang, Y., Wang, Z., Wenig, M., Wiegner, M., Wittrock, F., Xie, P., Xing, C., Xu, J., Yela, M., Zhang, C., Zhao, X., 2020. Intercomparison of MAX-DOAS vertical profile retrieval algorithms: studies on field data from the CINDI-2 campaign. Atmos. Meas. Tech. Discuss. https://doi.org/10.5194/amt-2019-456 (in review, 2020).

Toro, A.R., Seguel, R., Morales, S.R.E., Leiva, G.M., 2015. Ozone, nitrogen oxides, and volatile organic compounds in a central zone of Chile. Air Qual. Atmos. Health 8 (545–557), 1–13.

Vogelezang, D., Holtslag, A., 1996. Evaluation and model impacts of alternative boundary-layer height formulation. Bound. Layer Meteorol. 81, 245–269.

Von Schneidemesser, E., Monks, P.S., Allan, J.D., Bruhwiler, L., Forster, P., Fowler, D., Lauer, A., Morgan, W.T., Paasonen, P., Righi, M., Sindelarova, K., Sutton, M.A., 2015. Chemistry and the linkages between air quality and climate change. Chem. Rev. 115 (10), 3856–3897.

WMO, 2010. IV Tropospheric Ozone Analyzer Intercomparison. WCC-EMPA Report 10/5.

WMO, 2016. System and Performance Audit of Surface Ozone and Carbon Monoxide at the Global GAW Station Ushuaia, Argentina. WCC-EMPA Report 16/1.

WMO, 2017a. WMO Guidelines on the Calculation of Climate Normals. WMO-No. 1203 (ISBN 978-92-63-11203-3).

WMO, 2019. WMO Statement on the State of the Global Climate in 2018. WMO-No. 1233 (ISBN: 978-92-63-11233-0).

WMO, 2019b. WMO System and Performance Audit of Surface Ozone, Carbon Monoxide, Methane, and Carbon Dioxide at the Global GAW Station Ushuaia, Argentina, GAW Report No. 252, WCC-EMPA Report 19/3, 2019.

Worden, H.M., Deeter, M.N., Frankenberg, C., George, M., Nichitiu, F., Worden, J., Aben, I., Bowman, K.W., Clerbaux, C., Coheur, P.F., de Laat, A.T.J., Detweiler, R., Drummond, J.R., Edwards, D.P., Gille, J.C., Hurtmans, D., Luo, M., Martínez-Alonso, S., Massie, S., Pfister, G., Warner, J.X., 2013. Decadal record of satellite carbon monoxide observations. Atmos. Chem. Phys. 13 (2), 837–850.

Yela, M., Gil-Ojeda, M., Navarro-Comas, M., Gonzalez-Bartolomé, D., Puentedura, O., Funke, B., Iglesias, J., Rodríguez, S., García, O., Ochoa, H., Deferrari, G., 2017. Hemispheric asymmetry in stratospheric NO_2 trends. Atmos. Chem. Phys. 17, 13373–13389.

Zeng, G., Wood, S.W., Morgenstern, O., Jones, N.B., Robinson, J., Smale, D., 2012. Trends and variations in CO, C_2H_6, and HCN in the Southern Hemisphere point to the declining anthropogenic emissions of CO and C_2H_6. Atmos. Chem. Phys. 12 (16), 7543–7555.